Bow shock motions observed with CLUSTER

M. Maksimovic,[1] S. D. Bale,[2] T. S. Horbury,[3] and M. André[4]

Received 13 December 2002; revised 4 March 2003; accepted 11 March 2003; published 9 April 2003.

[1] The Cluster mission allows the determination not only of the bow shock crossing position but also, with a simple timing method and a reasonable confidence, the shock normal and the velocity along this normal. We apply this technique to a series of eleven consecutive bow shock crossings which occurred during a time interval of approximatively two and a half hours on 31 March 2001. We fit, on a distance versus time frame, the position of the bow shock subsolar point by imposing that the time derivatives at the crossings be equal to the shock speeds we determine. The curve we obtain this way represents global oscillations of the bow shock with a typical amplitude that compares quite well to the prediction of standard gasdynamic models which take into account the upstream solar wind plasma conditions. *INDEX TERMS:* 2784 Magnetospheric Physics: Solar wind/magnetosphere interactions; 2724 Magnetospheric Physics: Magnetopause, cusp, and boundary layers; 7811 Space Plasma Physics: Discontinuities. **Citation:** Maksimovic, M., S. D. Bale, T. S. Horbury, and M. Andre, Bow shock motions observed with CLUSTER, *Geophys. Res. Lett.*, *30*(7), 1393, doi:10.1029/2002GL016761, 2003.

1. Introduction

[2] From large datasets of the position of Earth bow shock crossings it has been possible to determine an average bow shock location and shape and to study the variations of the latter as a function of the incident solar wind parameters [for instance *Fairfield*, 1971; *Filbert and Kellogg*, 1979; *Formisano*, 1979; *Slavin and Holzer*, 1981; *Cairns et al.*, 1995; *Peredo et al.*, 1995]. The four spacecraft Cluster mission allows also such a study as a large number of crossings occurred since the beginning of the mission in late 2000. However the new point with having four identical spacecraft with adequate spatial separations to study the bow shock is that one can not only determine the bow shock crossing positions but also reliable estimations of the shock normal and velocity of the shock along this normal.

[3] The objective of the present study is to look to the constraints that the shock normal and speed determinations can possibly put on the bow shock standard models. In section 2 we describe the Cluster measurements and method that we use to determine the shocks normals and speeds. In section 3 we deduce from our observations global oscillations of the bow shock with a typical amplitude that we compare to the prediction of standard gasdynamic models which take into account the upstream solar wind plasma conditions. Finally we give some concluding remarks and perspectives in section 4.

2. Cluster Observations

[4] We analyze observations obtained by Cluster during a time interval of approximately two and a half hours on 31 March 2001. During this time interval a series of eleven bow shock crossings occured along the Cluster trajectory. The locations of these crossings are given in Table 1. In Figure 1 the Flux Gate Magnetometer (FGM) [*Balogh et al.*, 1997] spin resolution magnetic field modulus is displayed for Cluster 3 (C3). The eleven bow shock crossings can be clearly seen on this figure. They are characterized by a sharp transition of the magnetic field amplitude between solar wind (≈30 nT) and magnetosheath (≈80 to 100 nT) values. For the ninth and tenth crossings at ≈19:20, the sharp discontinuity of the magnetic field is present only for C3. No crossings are observed on the other spacecraft. This means that in this case the shock moving in the earthward direction reaches the Cluster tetrahedron with approximately zero speed and then moves away from the spacecraft in the sunward direction. For this double crossing the speed is therefore zero, but the normal cannot be determined. However, as we need the normal determination to fully characterize the bow shock motions we use in that case the normal determined for the following shock crossing, at 19:45:34.

[5] For each of the nine remaining shock crossings, we compute the bow shock normals and velocity using a simple timing method. This method is based on the assumption that each of the four spacecraft crosses a locally planar discontinuity moving at a constant speed. Taking for instance C3 as the reference spacecraft, the normal **n** and speed along this normal V can be obtained by solving the following system of equations

$$(\mathbf{r_i} - \mathbf{r_3}) \cdot \frac{\mathbf{n}}{V} = (t_i - t_3) \quad (1)$$

where t_i is the time when the spacecraft C_i crosses the shock and r_i its positions at that moment. Equation (1) is solved in GSE coordinates, assuming that the spacecraft velocity along its trajectory is negligible compared to V. This assumption is checked afterwards.

[6] In order to determine precisely the time of the crossings, we use the high time resolution data (5 points per second) of the spacecraft floating potential Φ_{SC} measured by the Electric Fields and Waves (EFW) experiment [*Gustafsson et al.*, 1997]. Actually what EFW samples 5 times per second is the electric antenna probe to spacecraft potential, which is a good approximation of the negative of the spacecraft potential. This potential is the result of the

[1]LESIA & CNRS, Observatoire de Paris-Meudon, France.
[2]Space Sciences Laboratory, University of California, Berkeley, USA.
[3]Blackett Laboratory, Imperial College, London, UK.
[4]Swedish Institute of Space Physics, Uppsala division, Sweden.

0094-8276/03/2002GL016761$05.00

Table 1. Normal, Angle θ_{Bn} Between the Normal and the Upstream Magnetic Field, Shock Speed, a_s and b_s Determinations for the Entire Set of Crossings

Crossing time at C3	$(x, y, z)_{GSE}$ for C3 (R_E)	n_x, n_y, n_z GSE	V km/s	θ_{Bn} deg.	a_s R_E	b_s 0.01 × R_E^{-1}
1, 17:14:40	9.50,−1.45,8.99	0.956,−0.150,0.252	−63.9	85.0	10.90	1.68
2, 17:17:54	9.55,−1.48,8.99	0.944,−0.186,0.273	47.2	86.1	11.15	1.92
3, 17:35:44	9.84,−1.66,8.98	0.988,−0.118,0.099	−85.7	82.1	10.56	0.85
4, 17:38:35	9.89,−1.69,8.97	0.905,−0.255,0.339	18.5	86.0	12.03	2.56
5, 18:01:59	10.25,−1.92,8.95	0.941,−0.264,0.211	−14.9	88.8	11.90	1.96
6, 18:28:24	10.64,−2.18,8.90	0.948,−0.198,0.248	29.0	82.2	12.18	1.82
7, 18:48:13	10.93,−2.38,8.86	0.913,−0.379,0.151	−30.1	57.6	12.99	2.43
8, 19:00:46	11.12,−2.51,8.83	0.977,−0.168,0.133	118.1	64.4	12.13	1.20
9 & 10, 19:19:30	11.38,−2.69,8.78	0.977,−0.093,0.191	0	64.1	12.39	1.18
11, 19:45:34	11.73,−2.94,8.70	0.977,−0.093,0.191	−95.0	64.1	12.74	1.18

Note that -V correspond to Earthward motion of the shock.

spacecraft charging due to expelled photoelectrons and impacting electrons and ions from the ambient plasma. Φ_{SC} value depends primarily on the ambient plasma density and can be used as a rough estimate of this parameter [*Pedersen et al.*, 2001].

[7] For each of the shock crossings, we determine the time differences $t_i - t_3$, needed to solve equation (1), in the following way: the time derivative of Φ_{SC} for spacecraft pairs (i, 3) are cross-correlated as a function of a time lag. The time lag which corresponds to the peak of the cross-correlation is then used as the optimal time shift. In Figure 2 we show an example of a crossing with the corresponding determination of **n** and V. Table 1 summarizes the normal, angle θ_{Bn} between the normal and the upstream magnetic field and speed determinations for the entire set of crossings. All the shocks are highly quasi-perpendicular. The shock velocities range roughly between 15 km/s and 120 km/s. As assumed initially, these values are much larger than the spacecraft velocity along its trajectory.

[8] Finally it should be mentioned that the shock normals and velocities we determine in the present study are very similar to those obtained by *Horbury et al.* [2002], who determined the crossing times by applying a similar technique to the magnetic field data. The mean and variance of the difference between our determinations of θ_{Bn} and those of *Horbury et al.* [2002] are 2.9° and 0.7° respectively. For the shock velocities, the corresponding mean and variance of the differences are 3 km/s and 1.9 km/s respectively.

3. Bow Shock Motions in Response to Solar Wind Plasma Conditions

3.1. Bow Shock Motions From the Cluster Measurements

[9] It is commonly assumed [*Fairfield*, 1971; *Filbert and Kellogg*, 1979; *Cairns et al.*, 1995] that the bow shock surface can be represented by a paraboloid:

$$x = a_s - b_s\left(y^2 + z^2\right) \tag{2}$$

where x, y, z are the GSE coordinates of a point at the surface, a_s is the standoff distance ($y = z = 0$) and b_s is the "flaring" parameter (for $x = 0$, $L = (y^2 + z^2)^{1/2} = (a_s/b_s)^{1/2}$).

[10] It can be easily shown that, using equation (2) to determine the orientation of the shock normal and setting the x-component of this normal to that observed, one

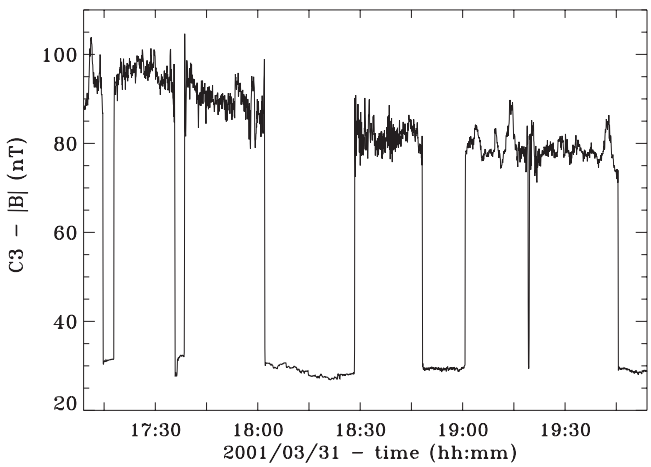

Figure 1. Cluster 3 spin resolution magnetic field magnitude (nT). Eleven bow shock crossings can be clearly seen, which are characterized by a sharp transition of the magnetic field amplitude between solar wind (≈30 nT) and magnetosheath (≈80 to 100 nT) values.

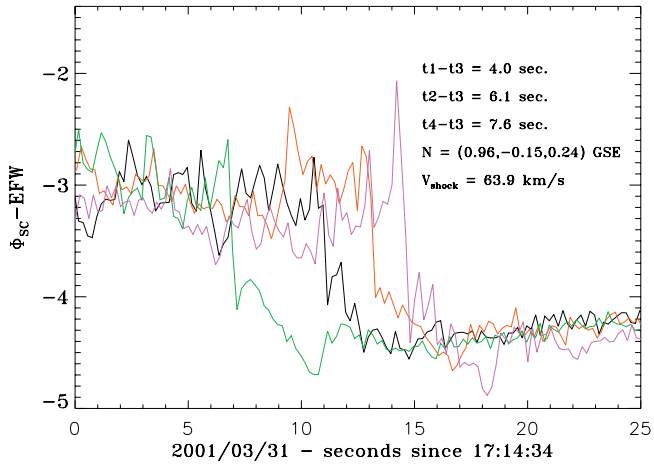

Figure 2. Example of a shock crossing observed with the Electric Fields and Waves experiment. The spacecraft floating potential Φ_{SC} is displayed for C1(black line), C2(red), C3(green), C4(magenta). The corresponding time differences and **n** and V determinations are indicated.

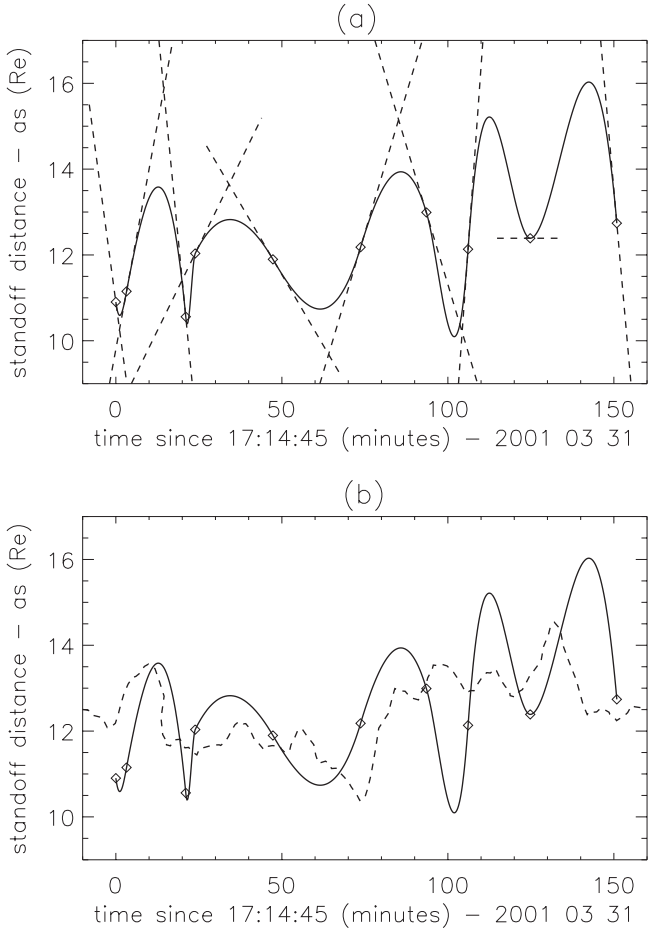

Figure 3. (a) The diamonds represent the standoff distance a_s obtained from the timing method and Cluster observations. The solid curve is obtained by computing a simple cubic polynomial which passes by all the a_{si} and for which the temporal derivatives at these points (dashed lines) are deduced from shock speeds determined with the timing method. (b) Superimposed to the variation of a_s deduced from the timing method and fitting (diamonds and solid curve), the dashed curve represents the temporal variation of the standoff distance deduced from the standard gas dynamic model (equation 2).

obtains, for each crossing i of our data set, the corresponding a_{si} and b_{si} from the following expressions:

$$a_{si} = x_i + \frac{\left(n_{yi}^2 + n_{zi}^2\right)^{1/2}\left(y_i^2 + z_i^2\right)^{1/2}}{2n_{xi}}; b_{si} = \frac{\left(n_{yi}^2 + n_{zi}^2\right)^{1/2}}{2n_{xi}(y_i^2 + z_i^2)^{1/2}}$$

where x_i, y_i, z_i are the positions of the shock crossings and n_{xi}, n_{yi} and n_{zi} are the components of the normals determined with the timing method. The values a_{si} and b_{si} we obtain for our set of crossings are given in Table 1.

[11] In Figure 3a we have displayed the standoff distance a_s we obtain for the set of crossings. In order to quantify the real variations of the standoff distance during the whole time period, we interpolate these points using the information provided by the determination of the instantaneous speed of the shocks that we measure. Since on average for the eleven bow shock crossings we have $b_{si} \times (y_i^2 + z_i^2) \ll a_{si}$, we can assume that $a_{si} \approx x_i$ and therefore $\partial a_{si}/\partial t \approx \partial x_i/\partial t = V_i n_{xi}$. The derivatives $\partial a_{si}/\partial t$ are indicated by the dashed lines on Figure 3a. Then for each pair a_{si}, a_{si+1}, we compute a simple cubic polynomial as a function of time which passes by a_{si} and a_{si+1} and for which temporal derivatives at these points are equal to $\partial a_{si}/\partial t$ and $\partial a_{si+1}/\partial t$ respectively. Thus the solid curve in Figure 3a is constructed by adding all together these segments of cubic polynomials.

3.2. Variations With Solar Wind Upstream Plasma Conditions

[12] Most of the commonly used models for the position of the bow shock and magnetopause subsolar point location are derived from *Spreiter et al.* [1966] gas dynamic simulations [*Sibeck et al.*, 1991; *Farris and Russell*, 1994; *Cairns et al.*, 1995; *Peredo et al.*, 1995; *Fairfield et al.*, 2001]. In these models, a_s is related to the subsolar point of the magnetopause a_{mp} by the expression $a_s = a_{mp} + a_{mp} \times \mathcal{F}(\gamma, M)$, where $\mathcal{F}(\gamma, M)$ is a function which actually represents the downstream to upstream density ratio of the shock. Also from *Spreiter et al.* [1966] gas dynamic simulations, and from the equality relation between the solar wind ram pressure P_{SW} and the inner magnetospheric magnetic pressure, it can be shown that the subsolar point of the magnetopause is related to P_{SW} by $a_{mp} = a_{mp0}\,(P_0/P_{SW})^{1/6}$.

[13] Taking the *Farris and Russell* [1994] form for the compression ratio and values for a_{mp0} and P_0 that are very close to the *Sibeck et al.* [1991] model, we use the following model for a_s:

$$a_s = 12.2\left(\frac{2}{P_{SW}}\right)^{1/6}\left[1 + 1.1\,\frac{(\gamma-1)M_A^2 + 2}{(\gamma+1)\left(M_A^2 - 1\right)}\right] \qquad (3)$$

where a_s is in R_E, P_{SW} is in nPa, $\gamma = 5/3$ and M_A is the Alfvén Mach number in the solar wind.

[14] We use the ACE-SWEPAM data to compute the temporal variations of the ram pressure and of the Alfvén Mach number in the solar wind. For this purpose we delay the ACE temporal series by the quantity D_{ACE}/V_{SW}, where D_{ACE} is the distance from ACE to the Earth and V_{SW} the ACE-SWEPAM solar wind bulk speed. We include the alpha particle densities in the determination of both the ram pressure and the Alfvén speed V_A. For the ram pressure computation, we assume that the alpha particles speed is $V_{SW} + V_A$ [*Marsch et al.*, 1982]. The temporal variation of the standoff distance deduced from ACE observations and equation 2 is represented on Figure 3b by a dashed line. It is superimposed on the value of a_s fitted from Cluster normal and speed determinations (solid line). For some sub-intervals of the period, the agreement between the two curves is relatively good, provided some slight time shifts are imposed between the two time series. However the important point of this comparison is the overall amplitude of the standoff distance variations. For a_s deduced from the Cluster observations, this amplitude is about 6 R_E. For a_s deduced from the standard model and the ACE solar wind conditions it is about 4 to 5 R_E.

4. Discussion and Perspectives

[15] The two main conclusions of the present study are the following: Firstly, the temporal variations of the bow shock

standoff distance deduced from the Cluster observations compare quite well with the variations of this parameter deduced from the classical gasdynamic models and the solar wind upstream plasmas conditions. Secondly, these variations are also comparable to the typical dispersion of the standoff distance deduced from the statistical studies based on large datasets (see for instance figure 2 in *Peredo et al.* [1995]). This means that the standard gasdynamlic model represented by equation (2) is not only valid on a statistical basis over a lot of crossings during long periods of solar wind variations. It is also valid on shorter time scales as the one we study here and which actually represent quite well the average variations of the solar wind plasma conditions.

[16] Numerous refinments can certainly be brought to the present study. First of all there is some evidence from the high resolution magnetic field profiles that there is an acceleration occuring while the shocks cross throught the Cluster tetrahedron [*Horbury et al.*, 2002]. If there is such an acceleration the shock speeds we measure with the simple timing technique and equation (1) are probably overestimated. Therefore the amplitude of the inferred standoff distance variations from CLUSTER measurements is also probably overestimated.

[17] There is also a timing issue due, on one hand, to the uncertainty of the delay introduced for the ACE time series and, on the other hand, to the typical time needed by the bow shock to respond to magnetopause variations [*Völk and Auer*, 1974]. This latter time could be estimated as being equal to the magnetosheath thickness in the subsolar direction divided by the Alfvén or magnetosonic speed. In the present case it is typically 2 to 3 minutes and probably can be neglected.

[18] Finally another point ought to be also mentioned. It is the fact that, during the time interval we study, the interplanetary magnetic field has a large negative southward component. B_z varies between -32 to -22 nT during the period. This large negative value could have impact on both the shape and the position of the magnetopause and consequently the bow shock (see for instance *Sibeck et al.* [1991] and references therein). This will be the purpose of a future study.

[19] **Acknowledgments.** We thank Catherine Lacombe for fruitful discussions and Dave McComas and Ruth Skoug for the use of the ACE SWEPAM data.

References

Balogh, A., et al., The Cluster Magnetic Field Investigation, *Space Sci. Rev.*, *79*, 65–92, 1997.

Cairns, I. H., et al., Unusual locations of the Earth's bow shock on September 24–25, 1987: Mach number effects, *J. Geophys. Res.*, *100*, 47, 1995.

Fairfield, D. H., Average and unusual locations of the Earth's magnetopause and bow shock, *J. Geophys. Res.*, *76*, 6700, 1971.

Fairfield, D. H., I. H. Cairns, M. D. Desch, A. Szabo, A. J. Lazarus, and M. R. Aellig, The location of low Mach number bow shocks at Earth, *J. Geophys. Res.*, *106*, 25,361–25,376, 2001.

Farris, M. H., and C. T. Russell, Determining the standoff distance of the bow shock: Mach number dependence and use of models, *J. Geophys. Res.*, *99*, 17,681, 1994.

Filbert, P. C., and P. J. Kellogg, Electrostatic noise at the plasma frequency upstream of Earth's bow shock, *J. Geophys. Res.*, *84*, 1369, 1979.

Formisano, V., Orientation and shape of the Earth's bow shock in three dimensions, *Planet. Space Sci.*, *27*, 1151, 1979.

Gustafsson, G., et al., The Electric Field and Wave Experiment for the Mission, *Space Sci. Rev.*, *79*, 137–156, 1997.

Horbury, T. S., et al., Four spacecraft measurements of the quasiperpendicular terrestrial bow shock: Orientation and motion, *J. Geophys. Res.*, *107*, 10.1029/2001JA000273, 2002.

Marsch, E., K. H. Muhlhauser, H. Rosenbauer, R. Schwenn, and F. M. Neubauer, Solar-Wind Helium-ions - observations of the Helios solar probes Between 0.3-au and 1-au, *J. Geophys. Res.*, *87*, 35–51, 1982.

Pedersen, A., P. Decreau, C.-P. Escoubet, G. Gustafsson, H. Laakso, P.-A. Lindqvist, B. Lybekk, A. Masson, F. Mozer, and A. Vaivads, Four-point high time resolution information on electron densities by the electric field experiments (EFW) on Cluster, *Ann. Geophys.*, *19*, 1483–1489, 2001.

Peredo, M., J. A. Slavin, E. Mazur, and S. A. Curtis, Three-dimensional position and shape of the bow shock and their variations with Alvnic, sonic and magnetosonic Mach numbers and interplanetary magnetic field orientation, *J. Geophys. Res.*, *100*, 7907–7916, 1995.

Sibeck, D. J., R. E. Lopez, and E. C. Roelof, Solar Wind flow control of the magnetopause shape, location, and motion, *J. Geophys. Res.*, *96*, 5489–5495, 1991.

Slavin, J. A., and R. E. Holzer, Solar Wind flow about the terrestrial planets, 1, Modeling bow shock position and shape, *J. Geophys. Res.*, *86*, 11,401, 1981.

Spreiter, J. R., A. L. Summers, and A. Y. Alksne, Hydromagnetic flow around the magnetosphere, *Planet. Space Sci.*, *14*, 223–253, 1966.

Völk, H. J., and R.-D. Auer, Motions of the Bow Shock Induced by Interplanetary Disturbances, *J. Geophys. Res.*, *76*, 40–48, 1974.

M. Maksimovic, LESIA, Observatoire de Paris-Meudon, F-92195, Meudon cedex, France. (milan.maksimovic@obspm.fr)

S. D. Bale, Space Sciences Laboratory, University of California, Berkeley, CA 94720-7450, USA.

T. S. Horbury, Blackett Laboratory, Imperial College, Prince Consort Road, London, SW7 2BW, UK.

M. André, Swedish Institute of Space Physics Uppsala Division, Box 537, SE-751 21, Uppsala, Sweden.